

# Development of Wet Tweezers Based on Capillary Force for Complex-Shaped and Heterogeneous Micro-Assembly

Ohmi Fuchiwaki, *Member, IEEE*, and Kazuya Kumagai

**Abstract**— In this paper, we have described newly developed wet tweezers based on capillary force for micro-assembly of complex-shaped objects. The tweezers are composed of two movable rods driven by a piezoelectric linear motor and two thin tubes. The two rods penetrate the liquids in the thin tubes. If we simply stamp the rods on a base, we can apply a drop of even high viscosity liquids. If we contact them to an object, we can pick it up by capillary force. Because we use the pair of the rods for picking up, posture of objects are fixed. That is important for accurate micro-assembly. To investigate generative force of the wet tweezers, we study relationship among viscosity, surface tension, and shape of meniscus of the liquid. We also formulate the capillary force as a function of gap distance between the rod and the object with three different liquids. In several experiments, we have confirmed the wet tweezers have good assembling accuracy and possibility to realize heterogeneous and complex-shaped micro-assembly.

## I. INTRODUCTION

Recently, miniaturization of portable devices and their electronic parts has been remarkable. Consequently, the need for micro manipulation to assemble more complex and smaller chip parts has been increasing. Conventional air-nozzle-based surface mounting technology (SMT) placement machines. They have various benefits, such as clean, fast, and high load capacity. However, these machines can only pick flat parts up. If the parts have complex shapes, they cannot pick up them because of air leaks, or posture error of the part occurs and their placement accuracy becomes worse. In table 1, we summarize characteristics of three typical pick-and-place methods, i.e. an air nozzle, a mechanical gripper, and capillary force. It is well known that, if size of objects is less than sub-millimeter, objects become sticky to the gripper and it is difficult to take them off because electrostatic force, an adhesive force, and the capillary force are stronger than force of gravity and inertia. There are many possibilities in micro-manipulation based on capillary force because electrostatic force is dampened very well if there is liquid between the object and the manipulator. The micro-manipulation based on the capillary force adapts to complex-shaped objects because the liquid changes its shape flexibly according to any shape of the contact surface [1, 2]. It also has great advantage for self-assembly because objects move toward a center of the liquid to minimize liquid's surface [3, 4]. However, posture of the object is easy to change by vibrations and inertia force because the liquid holds objects

Ohmi Fuchiwaki is with the Yokohama National Univ., 1-79 Tokiwadai, Hodogaya-ku, Yokohama, Kanagawa, Japan (phone: +81-45-339-3693; fax: +81-45-339-3693; e-mail: ohmif@ynu.ac.jp).

Kazuya Kumagai is with the Dept. of Mechanical Engineering, Yokohama National University (YNU).

loosely. If high-speed pick-and-place is required, we must feed the liquid drop to the rod fast and repetitively. There are two main feeding strategies which have proposed thus far as categorized in table 2. One is direct-control of a pressure of a liquid inside a thin tube [5, 6]. This method is good for quick feed for liquid drop. However, if the diameter of thin tube becomes less than 10 $\mu$ m, volume control of the drop is very difficult especially when the liquid has high viscosity, although the volume control is very important for controlling the capillary force. Another method is that simply dip the rod in the liquid as depicted in table 2. This method can change the drop size according to the diameter of the rod. However, the rod returns to the liquid every pick-and-place, so assembling efficiency is bad. Recently, we have developed a unique dispenser with single rod driven by a linear motor in z axis and a thin tube in which the liquid is trapped by capillary force. If the rod penetrates the liquid, the drop is fed to the rod automatically. When we simply stamp the wet rod on the base, the liquid drop is remained on the base as depicted in fig. 1. This method is well suitable for dispensing  $\mu$ m-sized drops, especially when the liquid has high-viscosity. Although,

TABLE I. COMPARISON OF CAPTURERING METHODS OF TINY OBJECTS

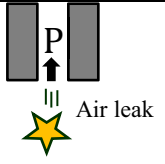

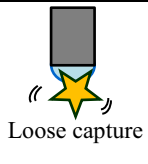
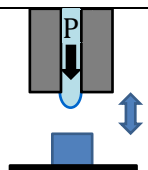
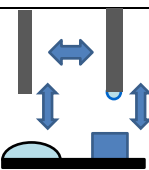
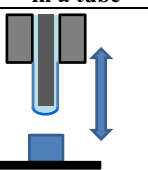
	Air nozzle	Mechanical gripper	Capillary force
Merit	Clean & Fast	Strong	Adapt to complex shape
Demerit	 Air leak	 Sticky	 Loose capture

TABLE II. FEEDING STRATEGY OF MICRO DROPS TO THE ROD

Method	Pressure control of liquid in a tube	One-by-one dip	Penetration of a rod into liquid in a tube
Principle			
Merit	Fast	Adapt to $\mu$ m-drop	Adapt to $\mu$ m-drop & Fast
Demerit	Not adapt to $\mu$ m-drop	Slow	Complex structure

conventional air-nozzle-based dispensers cannot dispense less than 100 $\mu\text{m}$  sized high-viscosity drops. In previous report, we have applied this dispenser for pick-and-place as depicted in figs. 2 and 3. In several experiments, we have succeeded in picking up various objects such as mm-sized metal ball, 0203 electronic chip parts, and  $\mu\text{m}$ -sized metal powder [7]. However, we could not fix postures of picked objects. That is the reason why we add one more rod to the manipulator for restricting the posture change as depicted in fig. 4. In this article, we report that achievements in developing the wet tweezers which has a pair of wet rods to hold objects tightly. In chapter 2, we explain modeling, design, and basic performance of the wet tweezers. In chapter 3, we characterize meniscus behavior of three different liquids. We also formulate the capillary force as a function of the gap distance between the rod and the base for each liquid to study influence of viscosity and surface tension to capillary force. In chapter 4, we show placement accuracy of rectangular plastic parts under various conditions. We also show placement accuracy of circular cones as one example of complex-shaped objects. We confirm that this method has enough feasibility to get sufficient placement accuracy for not only conventional flat chip parts but also heterogeneous complex-shaped objects. In chapter 5, we summarize contributions of this paper and discuss future works.

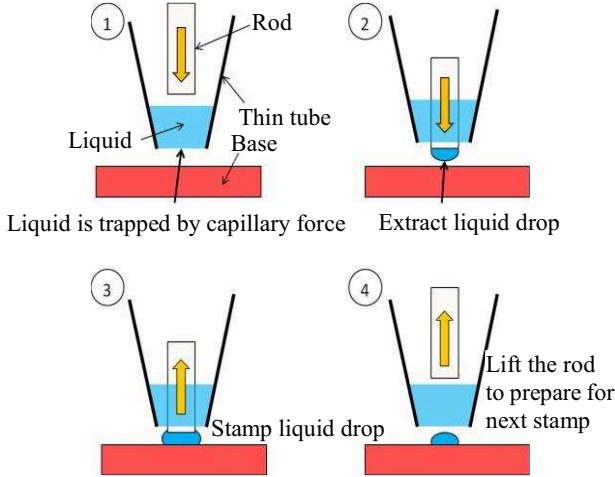


Fig. 1 Sequence of dispensing of drops with high viscosity

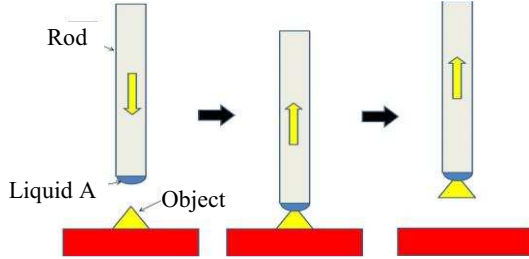


Fig. 2 Sequence of picking up by capillary force

## II. WET TWEEZERS

### A. Modeling in quasi-static condition

To simplify the problem, we consider the capillary-based pick-and-place by single rod in static equilibrium of forces. Fig. 5 illustrates forces acted on the target object when placing it down by single rod. Here,  $R_r$  is a radius of the rod.  $m$  and  $a$  are a mass and thickness of the object respectively.

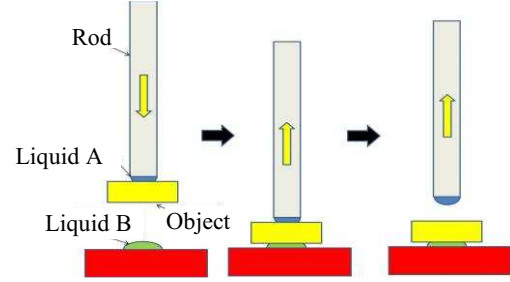


Fig. 3 Sequence of placing down

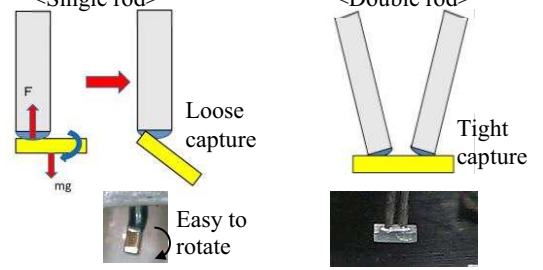


Fig. 4 Merit of capture by double rod

$L_A$  is a liquid sandwiched between the rod and the object.  $F_A$  is capillary force acting on top side of the object from  $L_A$ .  $H_A$  is a gap distance between the rod and the object.  $R_A$  is radius at a neck of meniscus of  $L_A$ .  $\rho_A$  is radius in  $r$ - $z$  plane at a neck of meniscus of  $L_A$ .  $\theta_A$  is contact angle of the meniscus on the top side of the object.  $\alpha_A$  is a slope angle of the meniscus at the edge of the rod. Note that  $\alpha_A$  is not a “contact angle” because surface of the rod is already wet; there are no triple line of the meniscus around the edge of the rod.  $\alpha_A$  is changeable according to other parameters.  $P_A$  is pressure inside  $L_A$ .  $\gamma_A$  is surface tension of  $L_A$ .  $F_B$ ,  $L_B$ ,  $H_B$ ,  $R_B$ ,  $\rho_B$ ,  $\theta_B$ ,  $\gamma_B$ , and  $P_B$  are defined in a similar way. Note that  $\alpha_B$  is a “contact angle”.  $z$  is height of the end of the rod from the base. It is well known that capillary force of  $F_A$  is sum of force caused by  $\gamma_A$  of cross sectional edge of  $L_A$  and force caused by pressure difference between  $L_A$  and air.  $F_B$  is represented in same way as given by,

$$F_A = -\pi R_A^2 \gamma_A \left( \frac{1}{R_A} - \frac{1}{\rho_A} \right) + 2\pi R_A \gamma_A \cong F_A(H_A). \quad (1)$$

$$F_B = -\pi R_B^2 \gamma_B \left( \frac{1}{R_B} - \frac{1}{\rho_B} \right) + 2\pi R_B \gamma_B \cong F_B(H_B). \quad (2)$$

Here, we suppose that  $R_A$  and  $\rho_A$  are functions of  $H_A$  approximately;  $F_A$  is represented as a function of  $H_A$  as (1). For the same reason,  $F_B$  is represented as a function of  $H_B$  as (2). From fig. 5, when the rod places the object down on the base, the force equilibrium is represented as given by,

$$F_A(H_A) \cong F_B(H_B) + mg. \quad (3)$$

Here,  $g$  is gravity acceleration. From fig. 5,  $z$  is represented as sum of  $H_A$ ,  $H_B$ , and  $a$  as given by,

$$z = H_A + H_B + a. \quad (4)$$

If  $L_B$  has higher viscosity and higher surface tension than those of  $L_A$ ,  $H_B$  and  $F_B(H_B)$  are approximately represented as constant value of  $h_B$  and  $f_B$  respectively as given by,

$$H_B \approx h_B = \text{const.} \quad (5)$$

$$F_B(H_B) \approx F_B(h_B) = f_B = \text{const.} \quad (6)$$

Substituting (5) and (6) into (3) and (4), we simplify the problem as given by,

$$F_A \approx F_A(H_A) \approx F_A(z - h_B - a) = f_B + mg. \quad (7)$$

$$H_A \approx z - h_B - a \quad (8)$$

From (7), we see that  $F_A$  is approximately represented as a function of  $z$ . When  $H_A$  is increased by increasing  $z$ , the object remains on the base because  $h_B$  is fixed. Positioning performance of  $z$  is very important to control  $F_A$ . We determine the positioning resolution is less than 100 nm and the measuring resolution is less than 50 nm to apply this method to heterogeneous micro-assembly from 5mm to 0.1 $\mu$ m. Higher velocity and acceleration are also important to get a better efficiency of the pick-and-place.

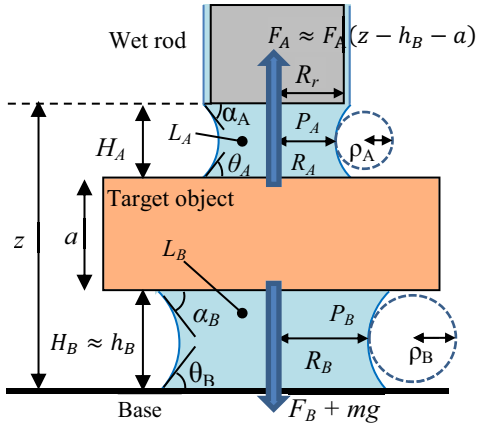


Fig. 5 Force equilibrium on the target object at placing down

### B. Mechanism design and basic performance

Fig. 6 shows a photograph of the mechanical dispenser for high-viscosity liquid with single rod. Fig. 7 shows the newly-developed wet tweezers for pick-and-place the object with a pair of the rods. The slider-A with the rods are driven by a piezoelectric linear motor (*P-664, PI*) in vertical axis along precise linear guide (*LS827, THK*) with measuring resolution of 20 nm of an optical linear encoder (*M3500, GSI*). The tubes are attached to the “passive” slider-B. The slider-B is connected to the slider-A by the double slider crank mechanism. Tables 3 and 4 show the performance of the linear motor and the linear encoder, respectively. Fig. 8 illustrates how to work the double slider crank mechanism which is designed for keeping the gap distance between the ends of the rods constant during one pick-and-place task. The rods push the tubes downward when the rods penetrate the

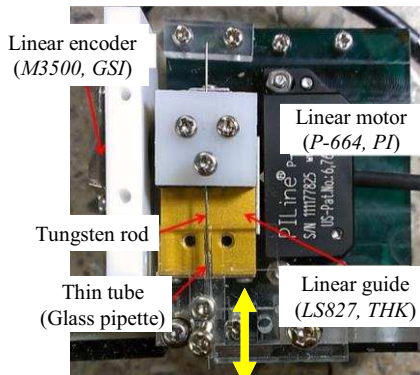


Fig. 6 Photograph of the dispenser for high-viscosity liquid

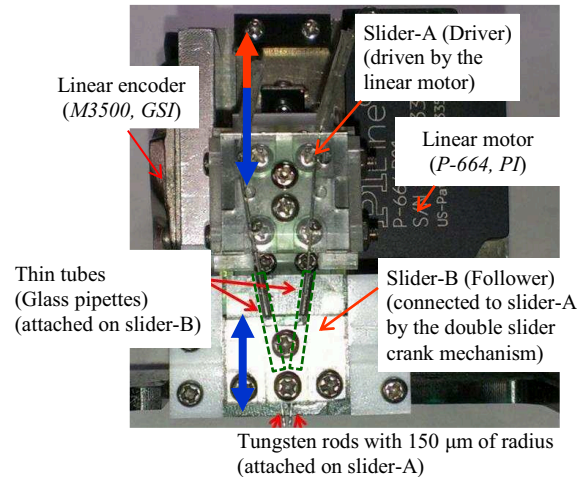


Fig. 7 Photograph of the newly fabricated wet tweezers

TABLE III. PERFORMANCE OF PIEZOELECTRIC LINEAR MOTOR (*P-664*)

Positioning resolution	50 nm
Maximum velocity	500 mm/s
Maximum acceleration	150 m/s <sup>2</sup>
Weight	10 g
Size	14 x 35 x 6 mm

TABLE IV. PERFORMANCE OF OPTICAL LINEAR ENCODER (*M3500*)

Measuring resolution	20 nm, (5 nm)
Maximum measuring velocity	576 mm/s, (114 mm/s)
Weight	5 g
Size	8 x 14 x 29 mm

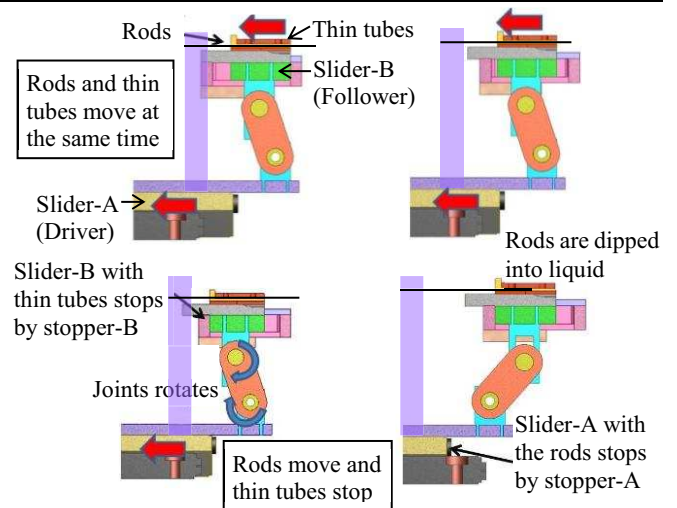


Fig. 8 Motion sequence of the double slider crank mechanism (side view)

tubes downward because the rods are arranged as V-shaped. Because this pushing force moves the passive slider-B, the rods and the tubes move simultaneously during one pick-and-place task. If the rods lift upward beyond the stopper-B, the passive slider-B stops at the stopper-B and the rods keep lifting until the end of the rods dip into the liquid.

### III. FORMULATION OF CAPILLARY FORCE

In previous section, we check that the gap distance of  $z$  is key parameter for controlling capillary force. In (1) and (2), we consider that  $R_A$  and  $\rho_A$  are functions of  $H_A$  approximately. Here, we describe geometry of meniscus of the three kinds of liquids to study influence of viscosity and surface tension to capillary force. We formulate capillary force as a function of the gap distance of  $H_A$ . We can easily get  $z$  from  $H_A$  as (8). There are numerous literatures which describe capillary force when a liquid is sandwiched between two ‘‘adhesional wetting’’ surfaces. However, ‘‘slope angle’’ of  $\alpha_A$  at the rod is not ‘‘contact angle’’.  $\alpha_A$  is just the slope angle of meniscus because there is no triple line around the rod.  $\alpha_A$  is easy to change, although contact angles of  $\theta_A$ ,  $\theta_B$ , and  $\alpha_B$  is constant during pick-and-place. In other words, we describe case study of the capillary force acted between spreading wetting surface of the rod and adhesional wetting surface of the base. That is unique condition and this is first article for considering that condition.

#### A. Experimental condition

We select an acrylic plate as the target object for picking up. We select water and two kinds of silicone fluids as the intermediate liquid between the rod and the base. In table 5, we show their surface tensions, kinematic viscosities, and contact angles on the acrylic plate. Water has largest surface tension and smallest kinematic viscosity in them. The two silicone fluids have different kinematic viscosity of 300cs and 1000cs. To simplify the explanation, we omit subscript of  $A$  from all parameters, i.e.  $H_A$  to  $H$ . We define kinematic viscosity as  $\nu$ , and a height of a neck of the meniscus from the base as  $H_n$ . We have used the tungsten rod with  $150\mu\text{m}$  of radius, so  $R_r$  is  $150\mu\text{m}$ .

TABLE V. CHARACTERISTICS OF THREE LIQUIDS

	Surface tension ( $\gamma$ )	Kinematic viscosity ( $\nu$ )	Contact angle ( $\theta$ )
Water	0.073 N/m	1 cSt	43.6 deg.
Silicone fluid with 300cs (KF96-300cs, Shinetsu)	0.021 N/m	300 cSt	45.7 deg.
Silicone fluid with 1000cs (KF96-1000cs, Shinetsu)	0.021 N/m	1000 cSt	41.2 deg.

#### B. Water

Water has 3.5 times *surface tension* and less than 1/300 times kinematic viscosity compared with other two silicone fluids. So, we consider water as a sample case that  $\mu$  is negligibly small and  $\gamma$  is strong. As shown in figs. 9 and 10, shape of its meniscus becomes circular arch when  $\rho + R < R_r$ , because strong surface tension squeeze meniscus to decrease its surface area and slight viscosity force resists that squeezing deformation. We see that there is donut-shaped flat area in the end of the rod. That is noted point of the meniscus of the water between surfaces of ‘‘spreading wetting’’ and ‘‘adhesional wetting’’. The rod is wet and there are neither  $\gamma_{SL}$  nor  $\gamma_{SV}$ ; pair of  $\gamma_{LV}$  is just pulling each other as depicted in fig. 10. In those conditions, the slope angle of  $\alpha$  at the upper beginning of the meniscus is 0 because one side of the liquid surface is flat and pair of  $\gamma_{LV}$  must be in a horizontal direction. At cross section of the neck,  $F$  is represented as given by,

$$F_C = -\pi R^2 \gamma \left( -\frac{1}{\rho} + \frac{1}{R} \right) + 2\pi R \gamma. \quad (9)$$

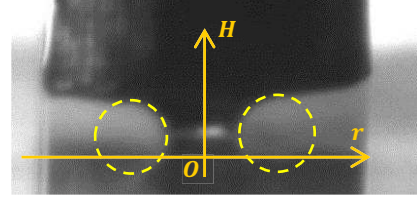


Fig. 9 Photograph of the meniscus of water

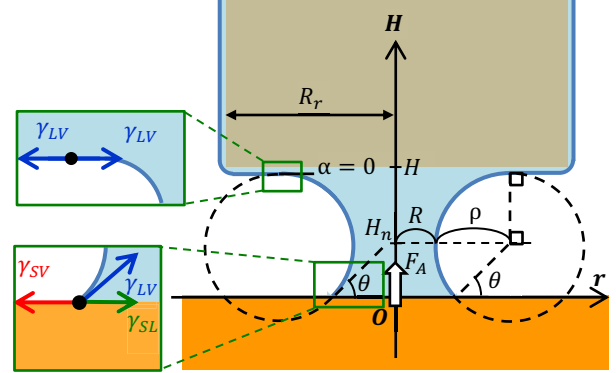


Fig. 10 Geometric model of the meniscus of water

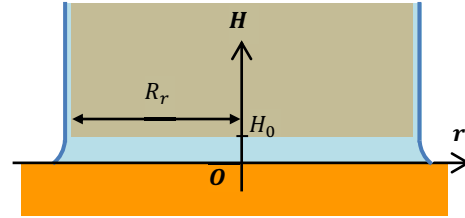


Fig. 11 Geometric model with  $H = H_0$

In fig. 10, we see,

$$H = \rho + R \sin \theta. \quad (10)$$

By substituting (10) to (9), we get

$$F = \pi \gamma R \left( R \frac{1 + \sin \theta}{H} + 1 \right). \quad (11)$$

If we consider additional condition of constant volume which is estimated by an approximate cylinder [2],

$$V = H_0 \pi R_r^2 \approx H \pi R^2. \quad (12)$$

Here,  $H_0$  is considered as boundary distance when the meniscus becomes cylinder shape with radius of  $R_r$ .

$$F(H) \approx \pi \gamma R_r \left( H_0 R_r \frac{1 + \sin \theta}{H^2} + \sqrt{\frac{H_0}{H}} \right). \quad (13)$$

Here, we estimate  $H_0$  by least square method (LSM) from experimental data. Due to space limitation, we omit equations to derive  $H_0$ . Note that we can represent  $F$  as a function of  $H$  because all other parameters are constant in (13). We can estimate the capillary force by (13) when  $H$  is larger than  $H_0$ . If  $H$  becomes smaller than  $H_0$ , we suppose that attracting force changes to repulsive force because the pressure inside liquid becomes positive. We use this formula as theoretical capillary force when liquid is water.

### C. Silicone fluid with 300cs

Silicone fluid with 300cs has smaller surface tension than water and smaller viscosity than silicone fluid with 1000cs. So, we consider silicone fluid with 300cs as a sample case of that both of  $\gamma$  and  $\mu$  are small. As shown in figs. 11 and 12, the shape of meniscus is well resembled to circular arch when  $\rho + R > R_r$ . There is not flat area of the rod's end in the meniscus because the surface tension is not enough to squeeze the meniscus until it makes the flat area. We have checked that the slope angle of  $\alpha$  varies according to  $H$ , so we have measured  $\alpha$  directly from image of the meniscus when we calculate its theoretical capillary force.

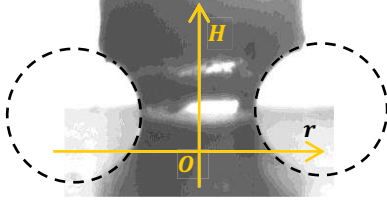


Fig. 11 Photograph of the meniscus of silicone fluid with 300cs

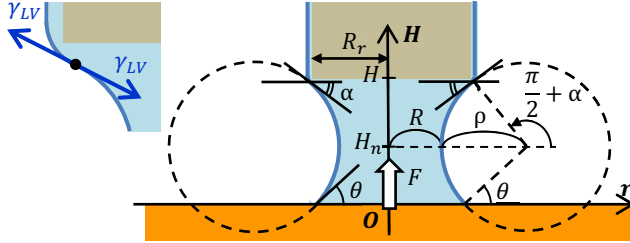


Fig. 12 Geometric model of the meniscus of silicone fluid with 300cs

From fig. 12,  $H$  is represented as given by,

$$H = \rho \sin\left(\frac{\pi}{2} + \alpha\right) + \rho \sin\theta. \quad (14)$$

If we consider additional condition of constant volume which is estimated by an approximate cylinder as given by,

$$V = H_0 \pi R_2^2 \approx H \pi \left(\frac{R + R_r}{2}\right)^2. \quad (15)$$

From (14), (15), and (9), we get the theoretical capillary force as a function of  $H$  and  $\alpha$  when  $H > H_0$ ,

$$F = \pi R_r \gamma \left\{ R_r (\cos\alpha + \sin\theta) \left( \frac{4H_0}{H^2} - \frac{4\sqrt{H_0}}{H^{\frac{3}{2}}} + \frac{1}{H} \right) + \frac{2\sqrt{H_0}}{\sqrt{H}} - 1 \right\}. \quad (16)$$

### D. Silicone fluid with 1000cs

Silicone fluid with 1000cs has smaller surface tension than water and larger viscosity than silicone fluid with 300cs. So, we consider silicone fluid with 1000cs as a sample case of that  $\gamma$  is small and  $\mu$  is large. As shown in figs. 13 and 14, the shape of the meniscus is close to a parabolic arch when  $\rho + R < R_r$ . We see that there is no flat area of liquid surface on the edge because the surface tension is not enough to squeeze the meniscus until it makes the flat area as the case of the silicone with 300cs. As the rod is lifted upward, the liquid is also lifted upward by the viscosity force because the upper side of the liquid is fixed to the rod. However, the liquid is also fixed the base and pulled downward by the viscosity force. The larger viscosity force is main reason why the meniscus becomes parabolic arch and the neck become thinner than that of the silicone with 300cs. We have checked that the slope angle of

$\alpha$  varies according to  $H$ . We have also see that sometimes we hardly determine  $\alpha$  because the slope around the edge changes complexly, so we have measured  $H_n$  from images of the meniscus instead of  $\alpha$  when we calculate its theoretical capillary force.

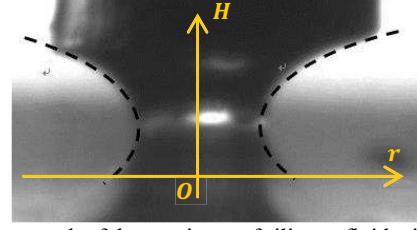


Fig. 13 Photograph of the meniscus of silicone fluid with 1000cs

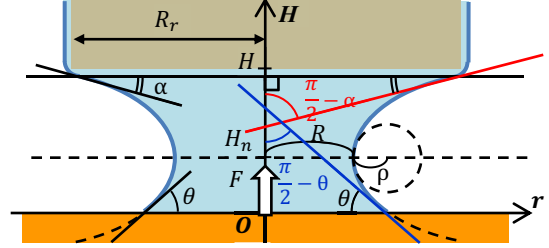


Fig. 14 Geometric model of the meniscus of silicone fluid with 1000cs

From fig. 14,  $R$  is represented as a function of  $H$  as given by,

$$R = R_r - \frac{(H - H_n)^2}{2H_n \tan\theta}. \quad (17)$$

While, radius of curvature of the parabolic arch at  $r=R$  is equal to  $\rho$  as given by,

$$\rho = H_n \tan\theta. \quad (18)$$

Substituting (17) and (18) into (9), we get the theoretical capillary force as a function of  $H$  and  $H_n$

$$F = \frac{\pi\gamma}{H_n \tan\theta} \left( R_r - \frac{(H - H_n)^2}{2H_n \tan\theta} \right) \left\{ \left( R_r - \frac{(H - H_n)^2}{2H_n \tan\theta} \right) + H_n \tan\theta \right\}. \quad (19)$$

### E. Comparison between theory and experimental results

As depicted in fig.15, we plot theoretical capillary force vs.  $H$ . We have controlled  $H$  by the single rod dispenser as shown in fig. 6 and captured the microscopic images every  $10\mu\text{m}$  from  $H=10\mu\text{m}$ . The meniscus of the water collapsed at  $H=90\mu\text{m}$ . That of the silicone fluid with 300cs collapsed at  $H=150\mu\text{m}$ . That of the silicone fluid with 1000cs collapsed at  $H=110\mu\text{m}$ . We have also measured maximum capillary forces 19 times for each liquid by an electric balance with  $10\mu\text{N}$  of measuring resolution as shown in fig. 16. In those experiments, we move  $H$  by manual stage with random velocity to investigate influence to the maximum force from dynamical condition. Error bars are standard deviation (SD) calculated from those 19 times measurements. From figs. 15 and 16, we see that water has largest capillary force, however SD is also largest. That means water's meniscus is easy to collapse by the dynamical condition. We see that silicone fluid with 1000cs is most reliable because the value of average minus SD is largest in those three. The silicone fluid with 300cs has smallest average force, however that is more reliable than water because the average minus SD is larger than that of water. We suppose that higher viscosity increases

robustness of the pick-and-place because the viscosity force prevents the meniscus from collapsing. We plan to measure  $F$ ,  $\rho$ , and  $R$  at every  $H$  simultaneously to check validity of (13), (16), and (19) in static condition. We also plan to investigate more detailed relationship among  $F$ ,  $H$ ,  $\dot{H}$ ,  $\gamma$ , and  $\mu$  by dynamic control of the single-rod dispenser of fig. 6 with 50 nm of positioning resolution.

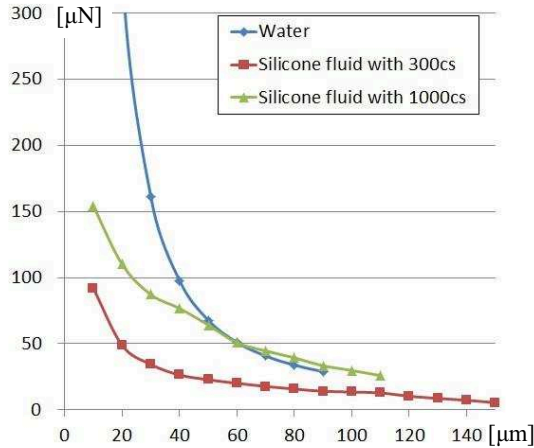


Fig. 15 Plots of theoretical capillary force vs.  $H$ . (Substituting measured value of  $H$ ,  $\alpha$ , and  $H_n$  to (13), (16), and (19))

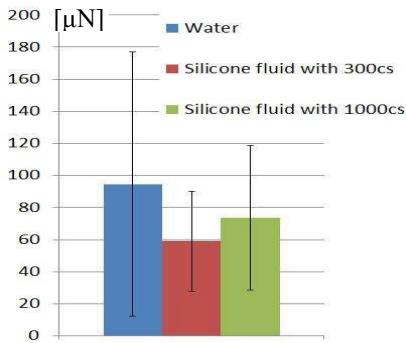


Fig. 16 Average maximum force with 19 times trial for each liquid with random velocity

#### IV. EXPERIMENTAL RESULTS OF PICK-AND-PLACE

##### A. Pick-and-place of rectangular acrylic parts

Fig. 17 shows experimental setup for pick-and-place. The target objects are acrylic rectangular parts, 1.5 x 1.0 x 0.5 mm, 0.5 mg, transparent color. The objects are made by same material of the base in chapter 3. The objects are placed on a rotational table driven by a stepping motor with rotational resolution of 0.002 degrees. The single-rod dispenser and the wet tweezers with a pair of the rods are fixed to coordinate system at rest. The stepping motor and a substrate on which we place the objects down are moved by XY linear stage with 1μm positioning resolution and bidirectional repeatability of positioning is ±0.5μm (YA10A-L1, Kozu). We have measured positions and postures of the objects by image analyzer (CV5700, Keyence) under microscopic observation with a CCD camera having 5M pixel (HV500M, Keyence). We have checked that the measuring accuracy is 7.1μm and 0.015degrees from statistical calculation of 200 times measuring with standard specimen of distance. We select the silicon fluid with 300cs as  $L_A$  for picking up, and the silicon fluid with 1000cs as  $L_B$  for placing down as shown in fig. 5. The rods diameters are 150μm, same as all other experiments.

We used single-rod-dispenser for applying  $L_B$ . We used both of the wet tweezers of fig. 7 and the single-rod-dispenser with  $L_A$  of fig. 6 for pick-and-place to compare the placement accuracy of them. Fig. 18 shows typical experimental results of the arrangements. There are some contaminations of  $L_B$  around the objects. However, we have succeeded in pick-and-place the objects by proposed method. Fig. 19 shows experimental results of average positioning errors and posture errors to show the comparison of placement accuracy between the single-rod and the wet tweezers (double-rod) methods. In these experiments, we placed the objects down on a double-stick tape. From fig. 19, both of average positioning error and its SD of the wet tweezers are about 50% of that of the single-rod method. Both of the average posture error and its SD of the wet tweezers are about 20% of that of the single-rod. Maximum posture error of the wet tweezers becomes 14% of that of the single rod. We have confirmed that the newly developed wet tweezers has better placement accuracy than that of the previous single-rod placement method. Applying patterns of  $L_B$  is one of main factors which determine the placement accuracy, so we have compared the

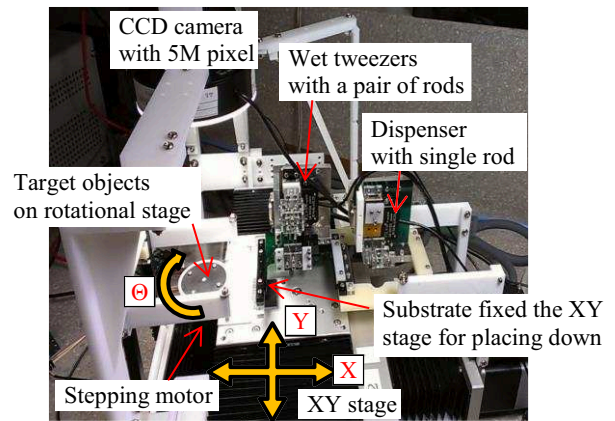


Fig. 17 Experimental setup

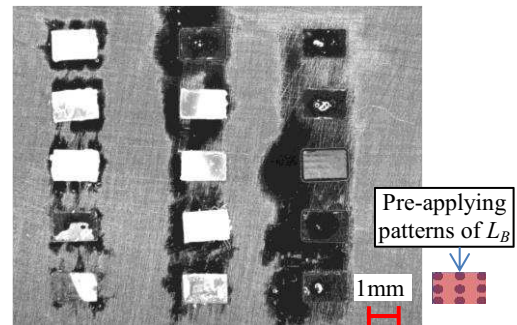


Fig. 18 Photograph of arrangement of rectangular plastic

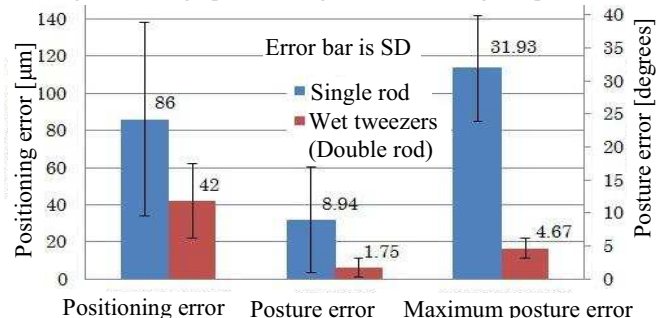


Fig. 19 Comparison of positioning and posture errors between the single-rod and the wet tweezers (double-rod) methods

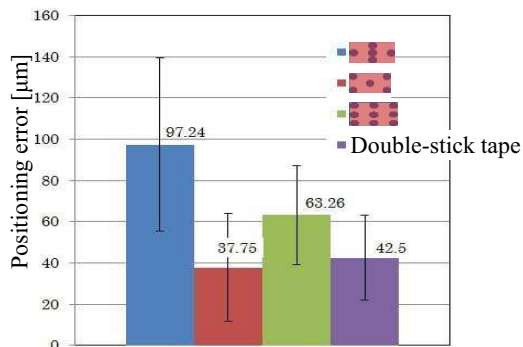


Fig. 20 Comparison of positioning errors among four kinds of applying patterns of  $L_B$  (pick-and-place by wet tweezers)

placement accuracy among three kinds of patterns as shown in fig. 20. We got minimum positioning error of  $38 \pm 14 \mu\text{m}$  (average  $\pm$  SD) when the applying pattern is the center-and-four-corners. This positioning error is same level of placement accuracy of conventional SMT placement machines. We confirmed that our proposed wet tweezers has much of feasibility for achieving sufficient placement accuracy for the practical use.

### B. Pick-and-place of circular cones

We select an acrylic circular cone with 0.8 mm in height and 1.5 mm in diameter as a sample of complex-shaped object. We conducted the pick-and-place of the circular cones under same conditions of the rectangular objects. Fig. 21 shows typical photographs of the placement. Fig. 22 shows experimental results of average positioning errors of the single-rod and the wet tweezers. From fig. 22, both of the positioning error and its SD of the wet tweezers are larger than that of the single-rod with positioning errors of  $94 \pm 70 \mu\text{m}$  (average  $\pm$  SD). This is because the posture is easy to change when the wet tweezers stick the lateral side of the cone as shown in fig. 23. The wet tweezers need to be positioned more precisely. While on the other hand, the single rod is just capture the top of the cone. Note that we didn't measure their posture errors because the cone is symmetrical about rotation. We plan to customize the ends of the rods according to shapes of target objects.

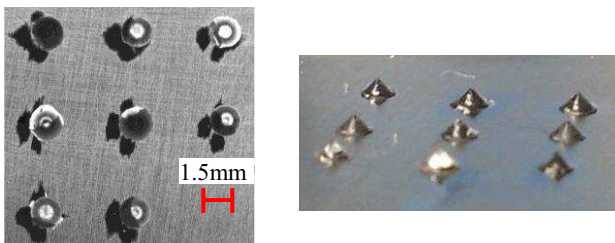


Fig. 21 Photograph of arrangement of tiny circular cones by the single-rod method

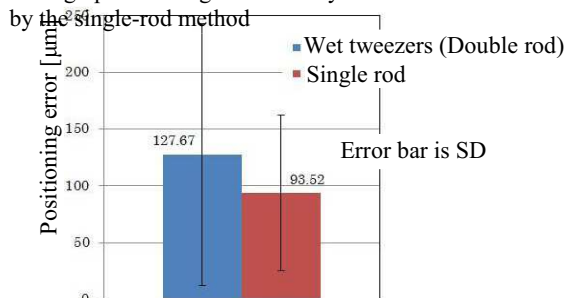


Fig. 22 Comparison of positioning error between the single-rod and the wet tweezers (double rod) of circular cones

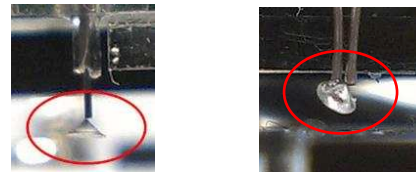


Fig. 23 Comparison of photographs of the circular cone between the single-rod and the wet tweezers during picking it up

## V. CONCLUSION AND FUTURE WORKS

We have described design and development of newly-proposed wet tweezers based on capillary force. The tweezers are composed of a pair of rods and a pair of thin tubes in which liquid is trapped by capillary force. We move the rods by linear motor with 50nm positioning resolution and 20nm measuring resolution. When the rods penetrate the liquids, the liquid drop is automatically fed on each of the two rods. The wet rods pick up target object by capillary force. The newly-developed wet tweezers are about 4 cm cubed and this is significantly compact compared with conventional air-nozzle based pick-and-place machine. Because the wet tweezers has a pair of the rods, posture of the flat object is more stable than previous single-rod method. There are three main contributions in this paper. First is proposing and developing the unique wet tweezers for fast pick-and-place of tiny objects by capillary force accurately. Second is study of meniscus deformation between "wet" rod and the adhesional base and formulation of capillary force as a function of the gap distance. This article is first one to consider that special condition. Third is that we have successfully conducted pick-and-place of mm-sized rectangular parts with average positioning error of  $38 \pm 14 \mu\text{m}$  (average  $\pm$  SD) and its posture error is  $1.75 \pm 1.5$  degrees. We have also conducted pick-and-place of circular cones with positioning errors of  $94 \pm 70 \mu\text{m}$ . We confirm the wet tweezers has good potential to realize compact, heterogeneous, and complex-shaped micro-assembly. We plan to check the validity of the proposed formulations of capillary force and develop dynamic control of the wet tweezers. We also plan to check placement accuracy of 0203 chip parts and  $\mu\text{m}$ -sized objects with complex shapes.

## REFERENCES

- [1] K. J. Obata, T. Motokado, S. Saito and K. Takahashi, scheme for micro-manipulation based on capillary force, *J. Fluid Mech.* (2004), vol. 498, pp.113-121.
- [2] *Capillary Forces in Micro assembly -Modeling, Simulation, Experiments, and Case Study*, P. Lambert, Springer, 2007
- [3] M. Mastrangeli, S. Abbasi, Ç. Varel, C. V. Hoof, C.P. Celis, K. F. Böhringer, Self-assembly from Milli to Nanoscales: Methods and Applications, *J. Micromech. Microeng.* (JMM), Vol. 19, No. 8, pp. 1-37, Topical Review (invited paper), 2009
- [4] J. Fang, K. F. Böhringer, Parallel micro component-to-substrate assembly with controlled poses and high surface coverage, *J. Micromech. Microeng.* (JMM) 16:721-730, pp.721-730, 2006
- [5] S. Koshimizu, Application of Liquid Bridging Force in Manipulation and Assembly of Microparts, *Int. J. of Automation Technology*, Vol.3, No.3, pp.308-312, 2009
- [6] H. Grutzeck, L. Kiesewetter, Downscaling of grippers for micro assembly, Springer, *Microsystem Technologies*, Vol.8, pp. 27-31, 2002
- [7] K. Kumagai and O. Fuchiwaki, Development of Dispenser for High-Viscosity Liquid and Pick & Place of Micro Objects Using Capillary Force, *j. of Key Engineering Materials*, Vol. 516, pp. 48-53, 2012